Optomechanically Induced Transparency

Stefan Weis, *et al.*

Science **330**, 1520 (2010);
DOI: 10.1126/science.1195596

Center funded by the U.S. Department of Energy (DOE), Office of Science, Office of Basic Energy Sciences (BES) under award DESC0001160. This work was performed in part at the Sandia-Los Alamos Center for Integrated Nanotechnologies (CINT), a U.S. DOE, Office of BES user facility. The LDRD supported the development and fabrication of platforms and the development of TEM techniques. The NEES center supported some of the additional platform development and fabrication and materials characterization. CINT supported the TEM capability and the fabrication capabilities that were used for the TEM characterization, and this work represents the efforts of several CINT users, primarily those with affiliation external to SNL. SNL is a multiprogram laboratory operated by Sandia Corporation, a wholly owned subsidiary of Lockheed Martin company, for the DOE's National Nuclear Security Administration under contract DE-AC04-94AL85000. The work of C.M.W. and W.X. was supported by the DOE Office of Science, Offices of Biological and Environmental Research, and was conducted in the Environmental Molecular Sciences Laboratory, a national scientific user facility sponsored by DOE's Office of Biological and Environmental Research and located at Pacific Northwest National Laboratory, which is operated by Battelle for the DOE under contract DE-AC05-76RLO1830. L.Q., A.K., and J.L. were supported by Honda Research Institute USA, Xi'an Jiaotong University, NSF grants CMMI-0728069, DMR-1008104, and DMR-0520020, and Air Force Office of Scientific Research grant FA9550-08-1-0325. S.X.M., L.Z., and L.Q.Z. were supported by NSF grants CMMI0825842 and CMMI0928517 through the University of Pittsburgh and SNL. L.Q.Z. thanks the Chinese Scholarship Council for financial support and Z. Ye's encouragement from Zhejiang University.

Supporting Online Material
www.sciencemag.org/cgi/content/full/330/6010/1515/DC1
Materials and Methods
Figs. S1 to S11
Movies S1 to S5
References

26 July 2010; accepted 26 October 2010
10.1126/science.1195628

Optomechanically Induced Transparency

Stefan Weis,[1,2]* Rémi Rivière,[2]* Samuel Deléglise,[1,2]* Emanuel Gavartin,[1] Olivier Arcizet,[3] Albert Schliesser,[1,2] Tobias J. Kippenberg[1,2]†

Electromagnetically induced transparency is a quantum interference effect observed in atoms and molecules, in which the optical response of an atomic medium is controlled by an electromagnetic field. We demonstrated a form of induced transparency enabled by radiation-pressure coupling of an optical and a mechanical mode. A control optical beam tuned to a sideband transition of a micro-optomechanical system leads to destructive interference for the excitation of an intracavity probe field, inducing a tunable transparency window for the probe beam. Optomechanically induced transparency may be used for slowing and on-chip storage of light pulses via microfabricated optomechanical arrays.

Coherent interaction of laser radiation with multilevel atoms and molecules can lead to quantum interference in the electronic excitation pathways (*1*). A prominent example observed in atomic three-level systems is the phenomenon of electromagnetically induced transparency (EIT), in which a control laser induces a narrow spectral transparency window for a weak probe laser beam. When this generic EIT effect had first been observed in an atomic gas (*2*), its relevance in nonlinear optics and optical (quantum) information processing was quickly recognized. In particular, the rapid variation of the refractive index concomitant with the opening of the transparency window gives rise to a dramatic reduction of the group velocity of a propagating optical pulse (*3*, *4*). Dynamic control of EIT with the control laser enables even a complete stop, that is, storage, of the pulse in an atomic medium (*5*, *6*). The experimental demonstration of slowing and stopping light (*3*–*6*) has attracted strong attention, because it provides a route to implement a photonic quantum memory (*7*) or a classical optical buffer. EIT has subsequently been studied in a wide variety of atomic media, but also in several solid-state systems (*8*, *9*) with a well-suited level structure.

Recent experiments with optomechanical systems have demonstrated that the mechanical response to thermal forces can be controlled by an optical field. This effect has been exploited, for example, to implement optomechanical laser cooling and amplification (*10*–*13*) as well as normal mode splitting (*14*). In other work, the mechanical response was optically tailored to exhibit destructive interference between different mechanical excitation pathways (*15*). Whereas in these studies, the mechanical response to thermal Langevin force was modified, we demonstrate here, as recently suggested (*16*, *17*), that the system's optical response to a weak "probe" laser can be controlled by a second "control" laser driving the lower motional sideband. A window of transparency arises from the destructive interference of excitation pathways for the intracavity probe field when a two-photon resonance condition is met. As pointed out independently, this effect can be considered a strict optomechanical analog of EIT (*18*), originating from a similar effective interaction Hamiltonian (*19*). Advantageously, this form of induced transparency does not rely on naturally occurring resonances and could therefore also be applied to previously inaccessible wavelength regions such as the technologically important near-infrared. Furthermore, a single optomechanical element can already achieve unity contrast, which in the atomic case is only possible within the setting of cavity quantum electrodynamics (*20*).

Our experiment (Fig. 1) consists of an optomechanical system featuring linear optomechanical coupling G in the sense that the cavity resonance frequency is given by $\omega_c'(x) = \omega_c + Gx$, where ω_c is the unperturbed resonance frequency. A control laser (frequency ω_l) maintains a control field $\bar{a}e^{-i\omega_l t}$, containing $|\bar{a}|^2$ photons, in the cavity. The static radiation pressure originating from this field displaces the mechanical mode by $\bar{x}$, leading to an effective detuning from the cavity resonance $\bar{\Delta} = \omega_l - (\omega_c + G\bar{x})$. We consider the situation where the control laser is tuned close to the lower motional sideband, i.e., $\bar{\Delta} \approx -\Omega_m$, where Ω_m is the mechanical (angular) resonance frequency. A second, weak laser oscillating at $\omega_p = \omega_l + \Omega$, is subsequently used to probe the (modified) cavity resonance by driving an intracavity probe field contained in a perturbation term $\delta a(t)$.

In the case of a weak probe field (compared to the control field), one can linearize the optomechanical dynamics (*21*) for the mechanical displacement $x(t) = \bar{x} + \delta x(t)$ and the intracavity field $a(t) = [\bar{a} + \delta a(t)]e^{-i\omega_l t}$ around the steady-state values $(\bar{x}, \bar{a})$. For the probe power transmission—that is, the ratio of the probe power returned from the system divided by the input probe power—the general expression

$$|t_p|^2 = \left| 1 - \frac{1 + if(\Omega)}{-i(\bar{\Delta} + \Omega) + \kappa/2 + 2\bar{\Delta}f(\Omega)} \eta_c \kappa \right|^2 \quad (1)$$

with

$$f(\Omega) = \hbar G^2 \bar{a}^2 \; \frac{\chi(\Omega)}{i(\bar{\Delta} - \Omega) + \kappa/2} \quad (2)$$

can be derived [see (*16*–*18*) and supporting online material (SOM) Eq. S25]. Here, $\chi(\Omega) = [m_{\mathrm{eff}}(\Omega_m^2 - \Omega^2 - i\Gamma_m\Omega)]^{-1}$ is the susceptibility of the mechanical oscillator of effective mass m_{eff} and damping rate Γ_m. The optical mode is characterized by a total loss rate $\kappa = \kappa_0 + \kappa_{ex}$ and the cavity coupling parameter $\eta_c = \kappa_{ex}/(\kappa_0 + \kappa_{ex})$. The presence of a control field $\bar{a}$ (tuned to the lower sideband) induces a transmission window for the probe beam when the resonance condition $\Omega \approx \Omega_m$ is met (Fig. 1). The depth and the width of this transmission window are tunable by the power of the control beam, as in the case of atomic EIT, with the best contrast achieved in the case of critical coupling $\eta_c = 1/2$.

To gain more physical insight into this phenomenon, it is instructive to consider this effect in a sideband picture. The simultaneous presence of control and probe fields generates a radiation-

[1]Ecole Polytechnique Fédérale de Lausanne, EPFL, 1015 Lausanne, Switzerland. [2]Max-Planck-Institut für Quantenoptik, Hans-Kopfermann-Strasse 1, 85748 Garching, Germany. [3]Institut Néél, 25 Rue des Martyrs, 38042 Grenoble, France.

*These authors contributed equally to this work.
†To whom correspondence should be addressed. E-mail: tobias.kippenberg@epfl.ch

pressure force oscillating at the frequency difference Ω. If this driving force oscillates close to the mechanical resonance frequency Ω_m, the mechanical mode starts to oscillate coherently, $\delta x(t) = 2\mathrm{Re}[X\, e^{-i\Omega t}]$. This in turn gives rise to Stokes- and anti-Stokes scattering of light from the strong intracavity control field. If the system resides deep enough in the resolved-sideband (RSB) regime with $\kappa << \Omega_m$, Stokes scattering (to the optical frequency $\omega_l - \Omega$) is strongly suppressed because it is highly off-resonant with the optical cavity. We can therefore assume that only an anti-Stokes field builds up inside the cavity, $\delta a(t) \approx A^-\, e^{-i\Omega t}$. However, this field of frequency $\omega_p = \omega_l + \Omega$ is degenerate with the near-resonant probe field sent to the cavity. Destructive interference of these two driving waves can suppress the build-up of an intracavity probe field. These processes are captured by the Langevin equations of motion for the complex amplitudes A^- and X, which require in the steady state (SOM Eqs. S26 and S27)

$$(-i\Delta' + \kappa/2)A^- = -iG\bar{a}X + \sqrt{\eta_c \kappa}\, \delta s_{in} \quad (3)$$

$$2m_{\mathrm{eff}}\Omega_m(-i\Delta' + \Gamma_m/2)X = -i\hbar G\bar{a}A^- \quad (4)$$

where δs_{in} is the amplitude of the probe field drive, and we abbreviate $\Delta' \equiv \Omega - \Omega_m$. We have assumed a high-quality factor of the mechanical oscillator ($\Gamma_m << \Omega_m$) and the control beam detuning $\bar{\Delta} = -\Omega_m$. The solution for the intracavity probe field amplitude reads

$$A^- = \frac{\sqrt{\eta_c \kappa}}{(-i\Delta' + \kappa/2) + \frac{\Omega_c^2/4}{-i\Delta' + \Gamma_m/2}}\delta s_{in} \quad (5)$$

This solution has a form well known from the response of an EIT medium to a probe field (*1*). The coherence between the two ground states of an atomic Λ system, and the coherence between the levels probed by the probe laser undergo the same evolution as do the mechanical oscillation amplitude and the intracavity probe field in the case of optomechanically induced transparency (OMIT). The role of the control laser's Rabi frequency in an atomic system is taken by the optomechanical coupling rate $\Omega_c = 2\bar{a}Gx_{\mathrm{zpf}}$, where $x_{\mathrm{zpf}} = \sqrt{\hbar/2m_{\mathrm{eff}}\Omega_m}$ designates the spread of the ground-state wave function of the mechanical oscillator. For $\Omega_c > \Gamma_m$, κ the system enters the strong coupling regime (*22*, *23*) investigated recently in the mechanical domain (*14*), in which the optical and mechanical systems are hybridized to dressed states that differ by $\hbar\Omega_c$ in their energy.

OMIT is realized using toroidal whispering-gallery-mode microresonators (Fig. 2A) (*10*, *17*). The cavity is operated in the undercoupled regime ($\eta_c < 1/2$), which together with modal coupling between counterpropagating modes (SOM Sec. 7) leads to a nonzero probe (amplitude) transmission $t_r = t_p(\Delta' = 0,\ \Omega_c = 0)$ at resonance (Fig. 2B), even in the absence of the control beam. In the case of the present device, $|t_r|^2 \approx 0.5$. [Note, however, that $|t_r|^2 < 0.01$ can be achieved with silica toroids (*24*).] To separate the effects of this residual transmission from OMIT, we introduce the normalized transmission of the probe $t_p' = (t_p - t_r)/(1 - t_r)$.

The mechanical motion was detected using a balanced homodyne detection scheme (fig. S1) measuring the phase quadrature of the field emerging from the cavity (*25*). This allows extracting the parameters of the device used in these experiments, which are given by (m_{eff}, $G/2\pi$, $\Gamma_m/2\,\pi$, $\Omega_m/2\,\pi$, $\kappa/2\,\pi$) ≈ (20 ng, −12 GHz/nm, 41 kHz, 51.8 MHz, 15 MHz), placing it well into the resolved sideband regime (*25*). To probe the cavity transmission spectrum in the presence of a control beam, the Ti:sapphire control laser is frequency modulated at frequency Ω using a broadband phase modulator, creating two side-

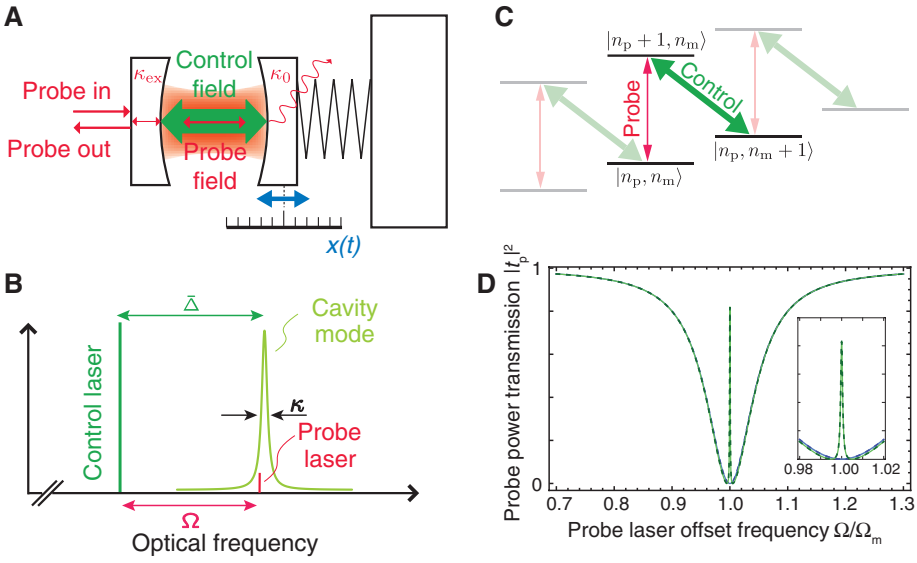

Fig. 1. Optomechanically induced transparency. (**A**) A generic optomechanical system consists of an optical cavity with a movable boundary, illustrated here as a Fabry-Perot–type resonator in which one mirror acts like a mass-on-a-spring movable along *x*. The cavity has an intrinsic photon loss rate κ_0 and is coupled to an external propagating mode at the rate κ_{ex}. Through the external mode, the resonator is populated with a control field (only intracavity field is shown). The response of this driven optomechanical system is probed by a weak probe field sent toward the cavity, the transmission of which (i.e., the returned field "Probe out") is analyzed here. (**B**) The frequency of the control field is detuned by $\bar{\Delta}$ from the cavity resonance frequency, where a detuning close to the lower mechanical sideband, $\bar{\Delta} \approx -\Omega_m$, is chosen. The probe laser's frequency is offset by the tunable radio frequency Ω from the control laser. The dynamics of interest occur when the probe laser is tuned over the optical resonance of the cavity, which has a linewidth of $\kappa = \kappa_0 + \kappa_{ex}$. (**C**) Level scheme of the optomechanical system. The control field is tuned close to red-sideband transitions, in which a mechanical excitation quantum is annihilated (mechanical occupation $n_m \rightarrow n_m - 1$) when a photon is added to the cavity (optical occupation $n_p \rightarrow n_p + 1$), therefore coupling the corresponding energy eigenstates. The probe field probes transitions in which the mechanical oscillator occupation is unchanged. (**D**) Transmission of the probe laser power through the optomechanical system in the case of a critically coupled cavity $\kappa_0 = \kappa_{ex}$ as a function of normalized probe laser frequency offset, when the control field is off (blue lines) and on (green lines). Dashed and full lines correspond to the models based on the full (Eq. 1) and approximative (Eq. 5) calculations, respectively.

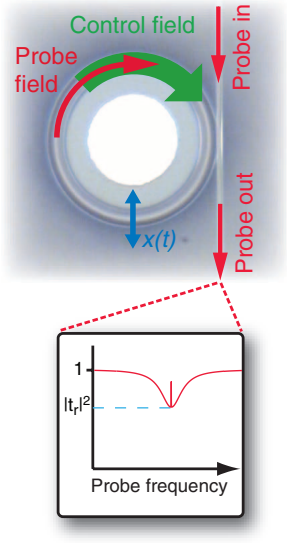

Fig. 2. Optomechanical system. (**Top**) A toroidal microcavity is used to demonstrate OMIT: The resonator is coupled to the control and probe fields using a tapered fiber. The optical mode couples through radiation pressure force to the mechanical radial breathing mode of the structure. In this ring geometry, the cavity transmission, defined by the ratio of the returned probe-field amplitude divided by the incoming probe field is simply given by the transmission through the tapered fiber. (**Bottom**) Under the chosen waveguide-toroid coupling conditions, there is a nonzero probe power transmission $|t_r|^2$ at resonance. The control field induces an additional transparency window with a contrast up to $1 - |t_r|^2$.

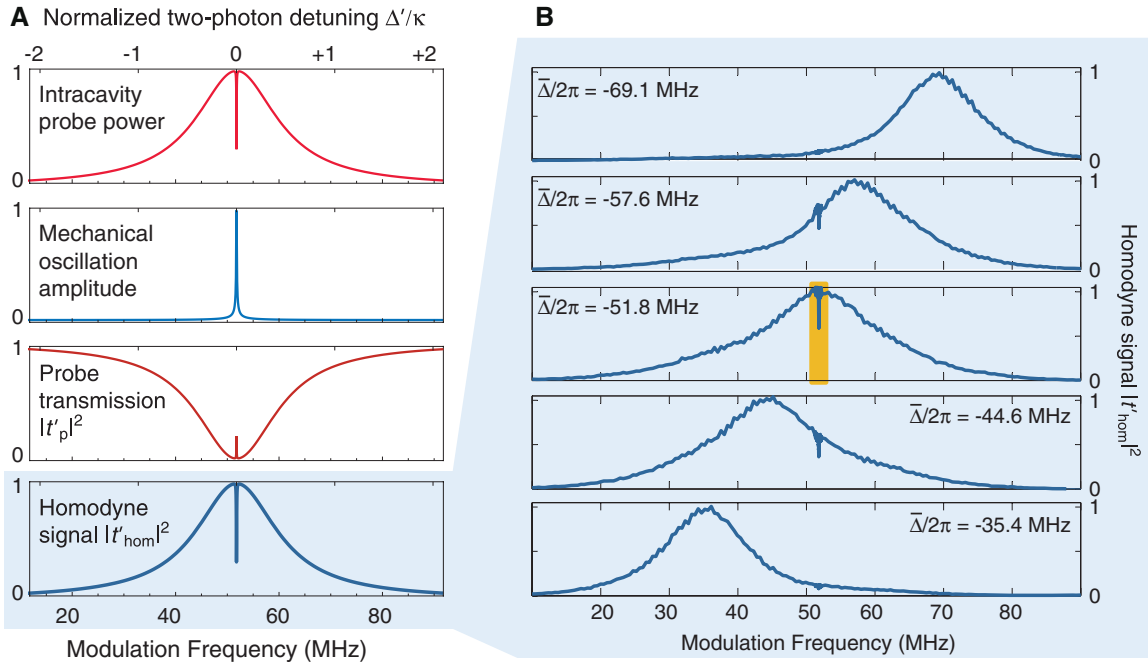

Fig. 3. Observation of OMIT. (**A**) Theoretically expected intracavity probe power, oscillation amplitude *X*, normalized probe power transmission $|t'_p|^2$, and the normalized homodyne signal $|t'_{hom}|^2$ as a function of the modulation frequency $\Omega/2\pi$ (top to bottom panels). The first two panels have additionally been normalized to unity. When the two-photon resonance condition $\Delta' = 0$ is met, the mechanical oscillator is excited, giving rise to destructive interference of excitation pathways for an intracavity probe field. The probe transmission therefore exhibits an inverted dip, which can be easily identified in the homodyne signal. (**B**) Experimentally observed normalized homodyne traces when the probe frequency is scanned by sweeping the phase modulator frequency Ω for different values of control beam detuning $\bar{\Delta}$. Whereas the center of the response of the bare optical cavity shifts correspondingly, the sharp dip characteristic of OMIT occurs always for $\Delta' = 0$. The power of the control beam sent to the cavity is 0.5 mW in these measurements. The middle panel shows the operating conditions where the control beam is tuned to the lower motional sideband $\bar{\Delta} \approx -\Omega_m = -2\pi \cdot 51.8$ MHz. The region around the central dip (orange background) is studied in more detail in a dedicated experimental series (see Fig. 4).

bands at $\omega_l + \Omega = \omega_p$ (probe field) and $\omega_l - \Omega$. In the resolved sideband regime, only the upper sideband, nearly resonant, interacts with the optomechanical system. Keeping the laser detuned to the lower motional sideband of the cavity ($\bar{\Delta} \approx -\Omega_m$), a sweep of the modulation frequency Ω scans the probe field through the cavity resonance. As shown in detail in the SOM (Sec. 5), demodulation of the total homodyne signal at the modulation frequency Ω using a network analyzer (NA) allows extracting a "transmission" homodyne signal t_{hom}, which, in the RSB regime, is related to the probe transmission by the simple relation $t_{hom} \approx 1 - t_p$.

Figure 3A shows the theoretically expected response of the optomechanical system and the detected signals. Clearly, the OMIT window is apparent in the intracavity probe power as described by Eq. 5, occurring simultaneously with the onset of radiation-pressure–driven mechanical oscillations. The excitation of the intracavity probe field therefore is suppressed, and the transmitted field nearly equals the probe field sent to the cavity. The lowest panel shows the corresponding homodyne signal, and the five panels in Fig. 3B show experimentally measured homodyne traces for detunings $\bar{\Delta}/2\pi$ varying from −69.1 MHz to −35.4 MHz and a control laser power of 0.5 mW. The center of the probe extinction (maximum of the homodyne signal) always occurs for $\Omega \approx -\bar{\Delta}$, because the probe laser then matches the cavity resonance [$\omega_p \approx \omega_c'(\bar{x})$]. Notably, however, the sharp OMIT window occurs only when the two-photon resonance condition $\Omega = \Omega_m$ (with $\Omega = \omega_p - \omega_l$) is met, independent of the detuning $\bar{\Delta}$ of the control beam, giving clear evidence to the theoretically suggested underlying mechanism.

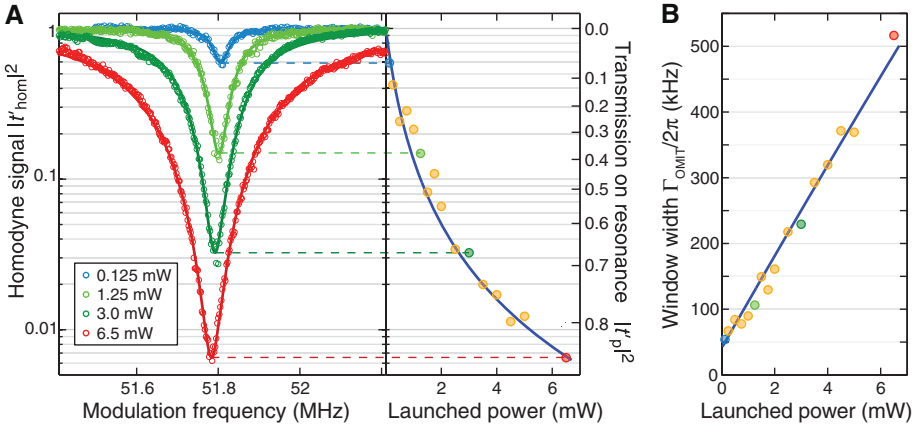

Fig. 4. Controlling OMIT. (**A**) Experimental normalized homodyne traces in the presence of a control beam (circles) for four different powers in the control beam from 0.125 mW up to 6.5 mW, and Lorentzian models. The minimum homodyne signal (measured at $\Delta' = 0$) directly indicates the maximum probe power transmission achieved in this case. These values are given in the right panel for a larger set of probe scans, together with the theoretical model developed in this work. (**B**) Width of the transparency window extracted from the same set of probe scans. Good agreement with the theoretical prediction is found over the entire power range.

To analyze the effect of the control beam more systematically, its detuning was fixed to the lower motional sideband. Varying its power from 0.125 to 6.5 mW, traces of the homodyne signal are taken in the vicinity of the two-photon resonance (Fig. 4). Dips of increasing depth and width are observed, which can be modeled by a simple Lorentzian function (SOM Sec. 3). The minimum homodyne signal is obtained under the condition of the two-photon resonance $\Delta' = 0$. In this case, the homodyne signal power and the probe power transmission are simply interrelated by $|t'_p|^2 = (1 - |t'_{hom}|)^2$, where $t'_{hom} = t_{hom}/(1 - t_r)$ is the normalized homodyne signal. The width

of the measured dip in the normalized homodyne signal is equal to that of the coupling-induced transmission window $\Gamma_{OMIT} \approx \Gamma_m (1 + C)$, where $C \equiv \Omega_c^2/\Gamma_m\kappa$ is an equivalent optomechanical cooperativity parameter (*14*). From the model (Eq. 5), the expected probe transmission on resonance is simply given by $t_p'(\Delta' = 0) = C/(C + 1)$. Our data match these expectations well if we allow for a linear correction factor in the optomechanical coupling frequency Ω_c due to modal coupling (SOM Sec. 7) and losses in the fiber taper. We have reached probe power transmission $|t_p'|^2$ up to 81%, indicating the high contrast achievable in OMIT.

In fact, any optomechanical system reaching $C \gtrsim 1$ can realize an appreciable control-induced probe transmission, as desired, for example, in all-optical switches. Interestingly, the systems currently available reach $C \approx 1$ with only thousands (*26*) or even hundreds (*27*) of control photons in the cavity, and recently emerging integrated nano-optomechanical structures (*28*) may be able to further reduce this number. The resulting extreme optical nonlinearities could be of interest for both fundamental and applied studies.

The tunable probe transmission window also modifies the propagation of a probe pulse due to the variation of the complex phase picked by its different frequency components. Indeed, a resonant probe pulse experiences a group delay of $\tau_g \approx 2/\Gamma_{OMIT}$ in the regime $C \gtrsim 1$ of interest (SOM Sec. 6), a value exceeding several seconds in some available optomechanical systems (*29*). However, undistorted pulse propagation only occurs if the full probe-pulse spectrum is contained within the transparency window of the system. This restricts the effectiveness of such a delay due to the fixed delay-bandwidth product of $\tau_g\,\Gamma_{OMIT} \approx 2$. A cascade of systems may alleviate this shortcoming—the most interesting scenario being a large array of concatenated optomechanical systems, as suggested in the context of OMIT (*16*, *17*, *30*), and radio frequency/microwave photonics (*15*). The group delay could then be dynamically tuned while the probe pulse is propagating through the array. Such systems could be practically implemented in lithographically designed optomechanical systems both in the microwave (*27*) and optical (*31*) domain.

Note added in proof: After online publication of this work, OMIT has also been reported in microwave optomechanical systems by Teufel *et al*. (*32*).

References and Notes

1. M. Fleischhauer, A. Imamoglu, J. P. Marangos, *Rev. Mod. Phys.* **77**, 633 (2005).
2. K.-J. Boller, A. Imamoglu, S. E. Harris, *Phys. Rev. Lett.* **66**, 2593 (1991).
3. A. Kasapi, M. Jain, G. Y. Yin, S. E. Harris, *Phys. Rev. Lett.* **74**, 2447 (1995).
4. L. V. Hau, S. E. Harris, Z. Dutton, C. H. Behroozi, *Nature* **397**, 594 (1999).
5. D. F. Phillips, A. Fleischhauer, A. Mair, R. L. Walsworth, M. D. Lukin, *Phys. Rev. Lett.* **86**, 783 (2001).
6. C. Liu, Z. Dutton, C. H. Behroozi, L. V. Hau, *Nature* **409**, 490 (2001).
7. M. D. Lukin, A. Imamoglu, *Nature* **413**, 273 (2001).
8. A. V. Turukhin *et al*., *Phys. Rev. Lett.* **88**, 023602 (2002).
9. D. Brunner *et al*., *Science* **325**, 70 (2009).
10. T. J. Kippenberg, H. Rokhsari, T. Carmon, A. Scherer, K. J. Vahala, *Phys. Rev. Lett.* **95**, 033901 (2005).
11. A. Schliesser, P. Del'Haye, N. Nooshi, K. J. Vahala, T. J. Kippenberg, *Phys. Rev. Lett.* **97**, 243905 (2006).
12. O. Arcizet, P.-F. Cohadon, T. Briant, M. Pinard, A. Heidmann, *Nature* **444**, 71 (2006).
13. S. Gigan *et al*., *Nature* **444**, 67 (2006).
14. S. Gröblacher, K. Hammerer, M. R. Vanner, M. Aspelmeyer, *Nature* **460**, 724 (2009).
15. Q. Lin *et al*., *Nat. Photonics* **4**, 236 (2010).
16. A. Schliesser, Cavity optomechanics and optical frequency comb generation with silica whispering-gallery-mode microresonators, Thesis, Ludwig-Maximilians-Universität München (2009); http://edoc.ub.uni-muenchen.de/10940.
17. A. Schliesser, T. J. Kippenberg, in *Advances in Atomic, Molecular and Optical Physics*, Vol. 58, E. Arimondo, P. Berman, C. C. Lin, Eds. (Elsevier Academic Press, 2010), pp. 207–323.
18. G. S. Agarwal, S. Huang, *Phys. Rev. A* **81**, 041803 (2010).
19. J. Zhang, K. Peng, S. L. Braunstein, *Phys. Rev. A* **68**, 013808 (2003).
20. M. Mücke *et al*., *Nature* **465**, 755 (2010).
21. C. Fabre *et al*., *Phys. Rev. A* **49**, 1337 (1994).
22. F. Marquardt, J. P. Chen, A. A. Clerk, S. M. Girvin, *Phys. Rev. Lett.* **99**, 093902 (2007).
23. J. M. Dobrindt, I. Wilson-Rae, T. J. Kippenberg, *Phys. Rev. Lett.* **101**, 263602 (2008).
24. M. Cai, O. Painter, K. J. Vahala, *Phys. Rev. Lett.* **85**, 74 (2000).
25. A. Schliesser, O. Arcizet, R. Rivière, G. Anetsberger, T. Kippenberg, *Nat. Phys.* **5**, 509 (2009).
26. G. Anetsberger *et al*., *Nat. Phys.* **5**, 909 (2009).
27. C. A. Regal, J. D. Teufel, K. W. Lehnert, *Nat. Phys.* **4**, 555 (2008).
28. M. Eichenfield, R. Camacho, J. Chan, K. J. Vahala, O. Painter, *Nature* **459**, 550 (2009).
29. J. D. Thompson *et al*., *Nature* **452**, 72 (2008).
30. D. E. Chang, A. H. Safavi-Naeini, M. Hafezi, O. Painter, http://arxiv.org/abs/1006.3829 (2010).
31. M. Eichenfield, J. Chan, R. M. Camacho, K. J. Vahala, O. Painter, *Nature* **462**, 78 (2009).
32. J. D. Teufel *et al*.; http://arxiv.org/abs/1011.3067 (2010).

33. T.J.K. acknowledges financial support by the Max Planck Society, European Research Council Starting Grant (SiMP), the European Union's MINOS, a Marie Curie Excellence Grant, the Swiss National Science Foundation, National Centre of Competence and Research of Quantum Photonics, and the Defense Advanced Research Projects Agency. S.D. is funded by a Marie Curie Individual Fellowship.

Supporting Online Material

www.sciencemag.org/cgi/content/full/science.1195596/DC1
SOM Text
Figs. S1 to S3
References

26 July 2010; accepted 1 November 2010
Published online 11 November 2010;
10.1126/science.1195596

A Determination of the Cloud Feedback from Climate Variations over the Past Decade

A. E. Dessler

Estimates of Earth's climate sensitivity are uncertain, largely because of uncertainty in the long-term cloud feedback. I estimated the magnitude of the cloud feedback in response to short-term climate variations by analyzing the top-of-atmosphere radiation budget from March 2000 to February 2010. Over this period, the short-term cloud feedback had a magnitude of 0.54 ± 0.74 (2σ) watts per square meter per kelvin, meaning that it is likely positive. A small negative feedback is possible, but one large enough to cancel the climate's positive feedbacks is not supported by these observations. Both long- and short-wave components of short-term cloud feedback are also likely positive. Calculations of short-term cloud feedback in climate models yield a similar feedback. I find no correlation in the models between the short- and long-term cloud feedbacks.

Much of the global warming expected over the next century comes from feedbacks rather than direct warming from CO_2 and other greenhouse agents. Of these feedbacks, the most complex and least understood is the cloud feedback (*1*, *2*). Clouds affect the climate by reflecting incoming solar radiation back to space, which tends to cool the climate, and by trapping outgoing infrared radiation, which tends to warm the climate. In our present climate, the reflection of solar energy back to space dominates, and the net effect of clouds is to reduce the net flux of incoming energy at the top of the atmosphere (TOA) by ~20 W/m^2, as compared to an otherwise identical planet without clouds. The cloud feedback refers to changes in this net effect of clouds as the planet warms. If, as the climate warms, cloud changes further reduce net incoming energy, this will offset some of the warming, resulting in a negative cloud feedback. If, on the other hand, cloud changes lead to increases in net incoming energy, then the change will amplify the initial warming, resulting in a positive cloud feedback.

Climate models disagree on the magnitude of the cloud feedback, simulating a range of cloud feedbacks in response to long-term global warming from near zero to a positive feedback of 1 W/m^2/K (*3*, *4*). This spread is the single most important reason for the large spread in the climate

Department of Atmospheric Sciences, Texas A&M University, College Station, TX, USA. E-mail: adessler@tamu.edu